



PHASE LOCKED PIV MEASUREMENTS IN WAKE OF AN AUTOMOTIVE FAN MODEL

Kaushik SAMPATH¹, Sri Krishna UPPALURI¹, Joseph KATZ¹
Yoon Shik SHIN², Michael SORTOR²

¹ *Dept. of Mech. Eng., Johns Hopkins University, Baltimore, MD 21218, USA*

² *Robert Bosch LLC, 101 First Avenue, Waltham, MA 02451, USA*

SUMMARY

Two dimensional particle image velocimetry performed in an optically index matched facility follows the evolution of flow structures in the wake of an automotive fan. To maintain high resolution, nine sample areas were patched together to cover the entire blade wake. Data obtained in a meridional plane include mean and rms velocity distributions. They show the entrainment of the blade wake by the tip vortex, as well as the diffusion and attenuation of the vortex strength, entrainment speed and wake velocity deficit with axial distance. Turbulence levels are elevated in the vicinity of the tip vortex, within the blade wake, as well as behind the rotor blade hub, especially at the intersection of the blade wake with shear layer behind the hub.

INTRODUCTION

The complex turbulent flow generated by automotive cooling fans interacts with radiator wakes and contributes to system noise. The objective of our experimental effort has been to measure these flow structures, elucidate key phenomena, and provide a comprehensive benchmarking database for validating Large Eddy Simulations (LES) of these flows, which are aimed at predicting the noise. The present paper summarizes part of the results of these measurements, focusing on the mean flow and turbulence statistics in the near wake of the fan.

There is an enormous body of literature on flow measurements within and around turbomachines, too big to summarize in this document. An extensive summary of the various techniques that have been used over the years is provided by Uzol *et al.* (2007). Hotwire and LDV were used extensively in early years by e.g. Lakshminarayana *et al.* (1974, 1982), Dong *et al.* (1990), Wo *et al.* (1997), Furukawa *et al.* (1998), Strazisar (1984), Zaccaria *et al.* (1997), Woisetschlager *et al.* (2003), etc. Particle Image Velocimetry (PIV) has been adopted extensively for turbomachines over the last decade, as summarized by Raffel *et al.* (2007) and Woisetschlager (2008). In application of PIV for studying near blade flows, one encounters difficulties because of the complex geometry of the blades and reflections from the boundaries. Consequently, most prior implementations of PIV in turbomachines stay away from boundaries. Our group has introduced the application of optical index matching to address this problem, and has implemented it successfully to study flows in

turbomachines (e.g. Miorini *et al.* 2012, Uzol *et al.* 2002; Wu *et al.* 2011, 2012, Soranna *et al.* 2006, 2008, 2010), rough wall boundary layers (Hong *et al.* 2011, 2012, Talapatra & Katz 2012, 2013) and tree canopy flows (Bai *et al.* 2012, 2013).

In summarizing prior work that is relevant to the present paper, we confine the discussion to PIV measurements performed in axial-radial (meridional) planes behind axial turbomachines. Cotroni *et al.* (2000) were able to capture two generations of the helicoidal vortex system in a propeller wake. They also observed the interactions of the blade wake and hub separation regions with the tip vortex. Stereoscopic PIV measurements by Yoon & Lee (2004) characterized the wake tip vortex system behind an axial fan. They verified qualitatively the presence of a system of rotating velocity deficits in the wake of an automotive cooling fan, which was measured earlier by Morris *et al.* (1998) using hotwires. Later, Felli *et al.* (2006) used PIV in conjunction with in-flow pressure fluctuation measurements, and were able to identify different pressure signals due to the propagation of the blade wake and the tip vortex systems. They concluded that the tip vortex was the major contributor to pressure fluctuations, while far downstream, the hub separation region was a significant component. Roosenboom *et al.* (2009), performed PIV measurements to study the slipstream of an aircraft propeller, and were able to capture several generations of the wake-tip vortex system.

The present study involves application of PIV to resolve the flow and turbulence in the wake of an automotive fan. Data obtained at 10 phases equally spanning a blade passage enables us to observe the evolution of several wake and tip vortex phases. Details of the experimental facility, fan geometry, experimental setup and measurement parameters are discussed in the following section. Results presented in subsequent sections include phase averaged distributions of mean velocity, rms values of velocity fluctuations and circumferential vorticity. Interactions among the tip vortex, blade wake and hub separation region are demonstrated and discussed.

FACILITY, EXPERIMENTAL SETUP AND PROCEDURES

Two dimensional particle image velocimetry was performed in a specially built optically index-matched facility in the Turbomachinery lab at Johns Hopkins University, which is illustrated in Figure 1. The 30 cm diameter fan and its shroud with a 30 cm inner diameter and 70 cm outer diameter designed by Robert Bosch LLC are present inside an acrylic casing. The internal surface of this acrylic casing is circular, but its outer boundary contains five flat windows to facilitate application of optical measurement techniques, in particular stereo-PIV. The working fluid within this closed loop facility is an aqueous solution of NaI whose concentration, about 62% by weight, is adjusted to match the refractive index of acrylic of 1.49 (Bai & Katz 2014, Budwig 1994). As a result, the shroud and fan become almost invisible, making it possible to perform optical measurements at any location within and around the fan. The kinematic viscosity of this fluid is $1.1 \times 10^{-6} \text{ m}^2/\text{s}$.

A 20 hp (max), adjustable speed centrifugal pump is used for circulating the flow in the facility and for generating 'RAM' conditions. The fan is driven by a separate motor whose speed is controlled by a precision inverter and its torque is measured by an inline torque meter. At the exit from the pump, the pipe cross section expands from 147 mm to 700 mm. To prevent flow separation and maintain flow uniformity, the diffuser contains a series flow straighteners (honeycombs + wire meshes) and concentric conical surfaces. We have verified that this system indeed prevents flow separation, and generates a uniform flow in the 700 mm diameter pipe upstream of the fan model. This flow then passes through a turbulence grid, which is located two fan diameters upstream of the shroud. This grid consists of 12.7 mm diameter stainless steel pipes separated horizontally and vertically by 50.8 mm. Its purpose is to add a moderate turbulence level to the inflow to the fan and it could be replaced by a radiator model. The 70 mm section is 2.27 m (7.5 fan diameters) long, and the location of the fan and shroud in it are adjustable. For the present study, the fan is located 3.75

diameters downstream of the pipe entrance. At the exit from this section, the flow enters a PVC return line and then is circulated back into the pump. The return line is equipped with an acoustic travel time flow meter and a kiel probe. The acrylic casing also contains of a series of pressure taps, circumferentially distributed upstream and downstream of the shroud for measuring the pressure difference across the fan, ΔP_{fan} .

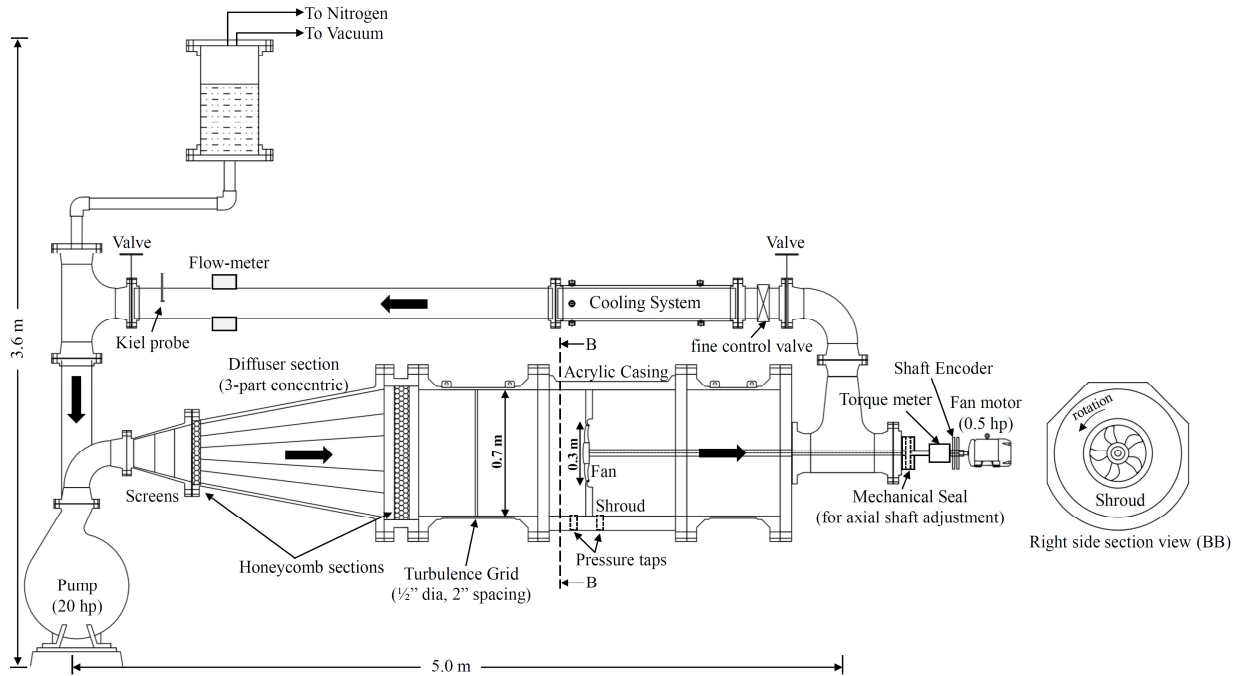


Figure 1: Left side view and right side cross section view of the fan facility at JHU

Relevant fan parameters are provided in Table 1. There are two operating conditions for this fan: in ‘IDLE’ condition the fan recovers pressure drop caused by a heat exchanger placed upstream when the vehicle is stationary, while in ‘RAM’ condition the vehicle is moving at 80 mph. The prescribed flow rates and fan rpm are scaled to match the Reynolds number based on tip speed of a 1:1 scale model operating in air. All experimental data presented in this study is for the RAM condition.

Table 1: Fan geometry and flow parameters

Fan diameter	[D]	302 mm
Number of blades	[n]	5
Tip chord length	[c]	43 mm
Tip clearance	[h]	3 mm
Tip speed	$[V_{tip}]$	3.04 m s^{-1}
Tip Reynolds number	$[Re_{tip}]$	1.19×10^5
Rotation speed	[N]	192.8 rpm
Flow rate (RAM condition)	[Q]	$0.0389 \text{ m}^3 \text{ s}^{-1}$
Static pressure rise (RAM condition)	$[\Delta P_{fan}]$	607 Pa

Since the slender fan blades are made of acrylic, they bend away (upstream) from the shroud when the fan rotates, causing an undesirable increase in the tip clearance beyond its design value. To address this problem a specially designed mechanical seal allows us to move the fan axially while it rotates. Since the blades are twisted in a complex way by design and consequently the blade shape changes as it bends, a simple translation such as the one achieved by the mechanical seal is not enough to recover the full design condition. Therefore, the fan blades have been “pre-compensated” to account for the bending and attain the right shape under the design flow conditions.

A series of separately performed experiments at Robert Bosch LLC were used for calibrating the bending of the blades under different flow conditions, allowing repeatable tip clearance regimes for the fan. These observations were also used to test the extent of blade vibrations, which appeared to stabilize as the tip clearance approached its design value of 3 mm.

For the pre-compensation, the fan was tested in a water tank to measure running deflections. A baffle was installed between the inlet and outlet of the fan to allow for regulating the pressure difference across the fan and to remove swirl from the inlet side flow of the fan. The fan leading and trailing edge positions were measured with a contact probe, consisting of a rod mounted on a movable stage for two radial stations. An accelerometer was mounted on the top end of the rod, with its output amplified and fed to headphones. At each measurement radius, the upper and lower surface deflections were measured separately at a series of rotation speeds. For each position measurement, the stage was adjusted until the contact between the rotating fan blade and the contact probe could be detected with the headphones. The probe position could then be read from the dial indicator. In order to confirm these measurements, an FEA analysis of the same operating conditions was run. Based on CFD results, it was decided to run the inverse deflection problem in FEA, in order to calculate a blade shape with inverse deflections of what was expected from the PIV operating loads. A reasonable agreement was reached between the experimental measurements and the computed model, and the final pre-compensated shape was determined. Once the acrylic fan was received and installed in the JHU facility, its axial location was adjusted during the experiment to achieve the specified tip clearance while the facility and fan were operating.

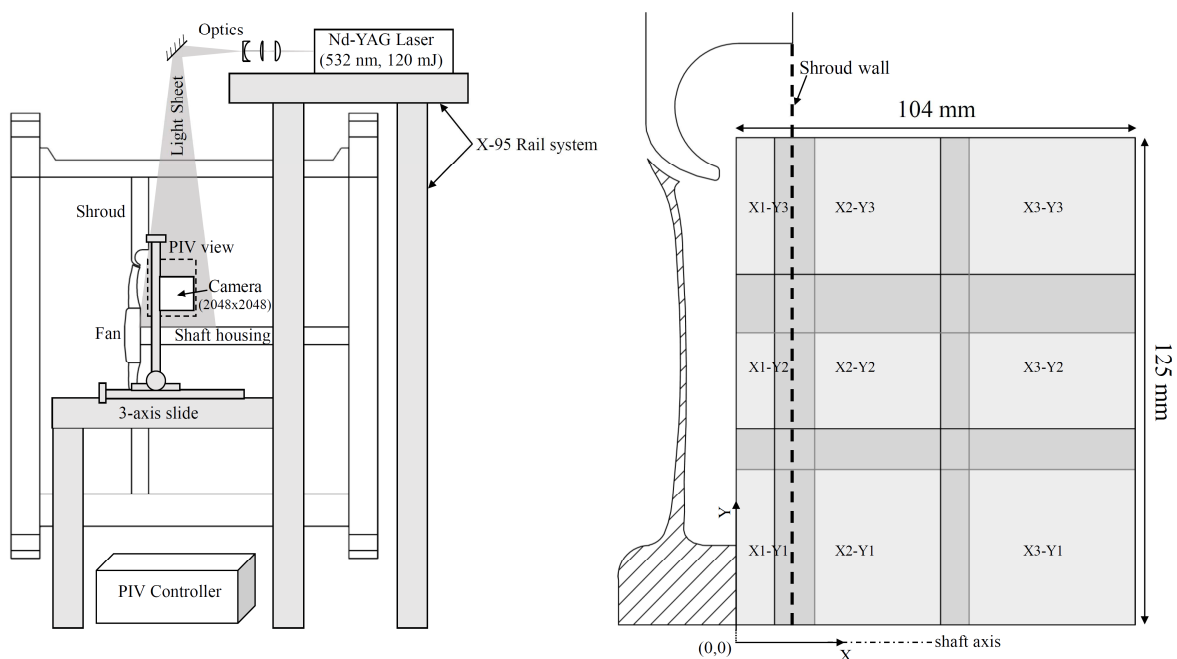


Figure 2: PIV system (left) and blade cross section (phase P1) positioned with PIV field of view (right).
 Field of view is split into 9 sample areas. X (axial) axis along the shaft center,
 while Y (radial) axis along the back face of the hub.

A schematic description of the PIV setup is provided in Fig 2. A 120 mJ/pulse Nd-YAG laser (532 nm) was used to illuminate the flow field seeded with 13 μm diameter silver coated hollow glass spheres. A 2048 \times 2048 pixel camera sensor with a 105 mm lens was used to record 1250-1500 image pairs for each location and phase. The shaft of the fan was coupled with an encoder consisting of two slotted discs, enabling us to track the exact phase of the fan for any blade. This encoder triggered the PIV controller firing the laser and camera in a timely manner allowing us to record phase locked PIV images for 10 blade phases separated equally by 7.2 $^\circ$ degrees, which spanned an entire single blade passage (Fig 3).

To adequately resolve turbulent flow structures in the wake, measurement resolution needed to be high, well below 1 mm. However, to capture the interaction among elements of the wake required a field of view that is comparable to the fan radius. Thus, the measurements had to resolve nearly three orders of magnitude of length scales. To address this problem in a phase-averaged sense, nine 50 \times 50 mm sample areas were patched together, with some overlap, to form a 105 \times 125 mm field of view in the axial-radial plane covering the entire wake of the fan. The final vector spacing was 0.39 mm (16 pixels). The field of view, sample areas and the overlap regions are shown with together with a sample blade cross section (phase P1) in Fig 3).

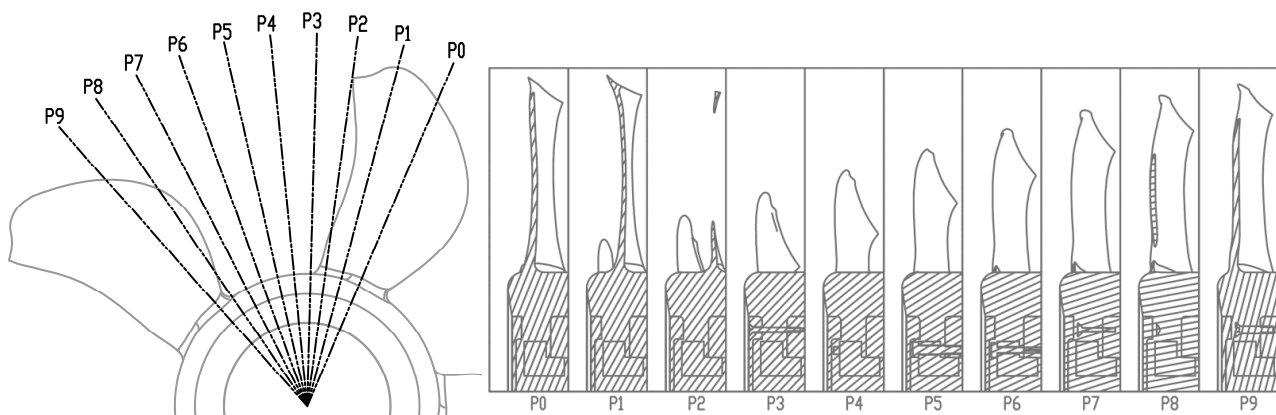


Figure 3: Front view of fan cut at ten radial planes (left) and cut sections of the phases (right).
Hatched portion represents the intersection of the blade with the light sheet.

The data analysis procedure comprised of three steps. First was image enhancement, where the intensities of particle traces were enhanced to achieve uniformity while removing the background noise. Background removal was performed by a threshold based mean intensity subtraction for each pixel. Particle enhancement was performed by multiple iterations of a modified histogram equalization (MHE) algorithm using an in house code (Roth & Katz 1999, 2001). PIV processing was carried out using ‘gauCorr’ – an in house cross-correlation code. The correlation box size varied depending on particle distributions over the field of view, from 0.78 \times 0.78 mm (32 \times 32 pix.) with 50% overlap between windows to 1.18 \times 1.18 mm (48 \times 48 pix.) with 66% overlap.

Owing to challenges caused by large velocity gradients in parts of the flow field, careful scrutiny of the processed results has been critical. First, overlapping regions between sample areas with redundant measurements served as validation, as these high gradient structures propagated through them across phases. Second, commercial PIV software, DaVisTM was utilized in parallel for some of the data analysis, using its deformable interrogation window feature for regions with high velocity gradients. The differences between results have been negligible. Third, an additional post-processing step was using to remove outliers in the data. These outliers could be detected spatially (Westerweel & Scarano 2005) and/or temporally. Since the particle image quality was expected to be consistent at a given location, we removed data points with sudden dips in the cross-correlation magnitude, while maintaining data whose correlation peak magnitude exceeded a local threshold level determined based on the rest of the data. For most of the data, at least 1000 instantaneous realizations were used to obtain phase averaged statistics of mean flow and turbulence level.

RESULTS AND DISCUSSION

In presenting the results, the coordinates (x, y) represent the axial and radial distances from the intersection of the back face of the hub and shaft center as shown in Fig. 2. The corresponding axial and radial instantaneous velocity components are u and v respectively. Their phase-averaged values are U and V ; the velocity fluctuations are denoted as u' and v' and their rms values are $\langle u'u' \rangle^{1/2}$ and $\langle v'v' \rangle^{1/2}$. All coordinates have been non-dimensionalized by the fan diameter (D), the velocities have been scaled by the tip speed (V_{tip}) and the mean circumferential vorticity $\Omega_\theta/N = (\partial V/\partial x - \partial U/\partial y)/N$ with the shaft rotational speed (N) in rad/s. Fig 4 shows sample 50×50 mm distributions of U and V to give the reader a sense of the actual data resolution superimposed on contour lines of mean vorticity. This sample focuses on structure of the tip vortex shortly after it enters the sample area. The enhanced streamwise velocity downstream of the vortex is already associated with the next structure, whose center is located downstream of the sample area. The region with elevated radial velocity at the bottom right hand corner of this sample, where the streamwise velocity is low, is part of the blade wake being entrained into the tip vortex.

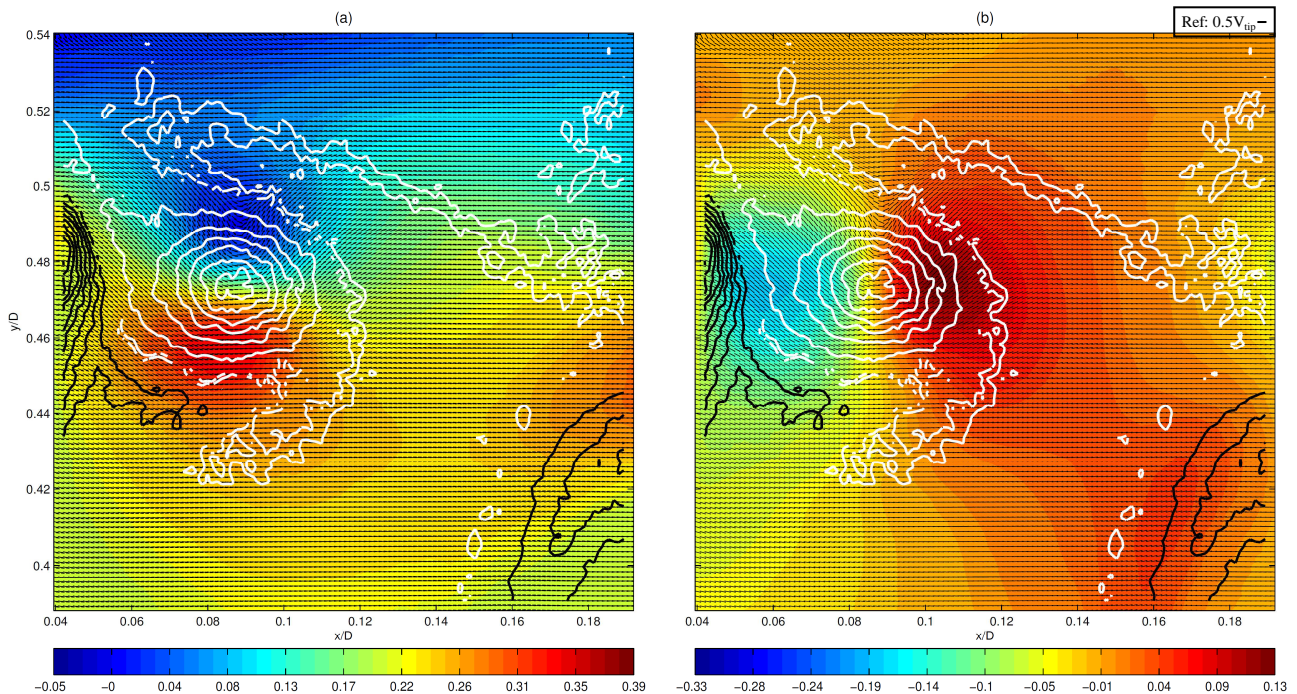


Figure 4: Color contours: Distributions of non-dimensionalized (using the tip speed) phase averaged (a) axial, and (b) radial velocity components for sample area X2-Y3 at phase P6. The vectors show the total velocity in full resolution with a reference vector provided on top. The line contours show distributions of Ω_θ/N (black <0 , white >0).

In Fig 5-9, the nine sample areas are combined to show, respectively, the distributions of streamwise and vertical velocity components, the streamwise and vertical rms values of velocity fluctuations, and the mean circumferential vorticity. The boundaries of the sample areas are clearly indicated, and we do not include overlapped data for clarity. After implementing the filtering methods discussed in the previous section, except for a few points with high velocity gradients, the differences between overlapped data fall below 6% for the mean velocity and 4% for the rms values. In figures 5 and 6, the vector densities are diluted by 10:1 for clarity. As we progress from phase P0 to P9, the blade is rotating out of plane towards the reader, and the main the flow is from left to right. The center of the blade dissects the PIV plane in phase P1 (Fig 3).

As one follows the flow development between phases, the progress of the helicoidal system, consisting of a series of tip vortices and blade wakes, as they interact with the hub separation region and among themselves, becomes clearly evident. The sample area covers three tip vortices generated by neighboring blades, all containing, as expected, positive (counter-clockwise) vorticity

(Fig. 9), which appears to diffuse as the structures move downstream. The wakes can be identified by streamwise velocity deficits and parallel layers with opposite sign circumferential vorticity. The latter are associated with the “jet” with positive radial velocity at the center of the wake resulting from entrainment of this wake by the tip vortex as seen in Fig 6 (further discussion follows).

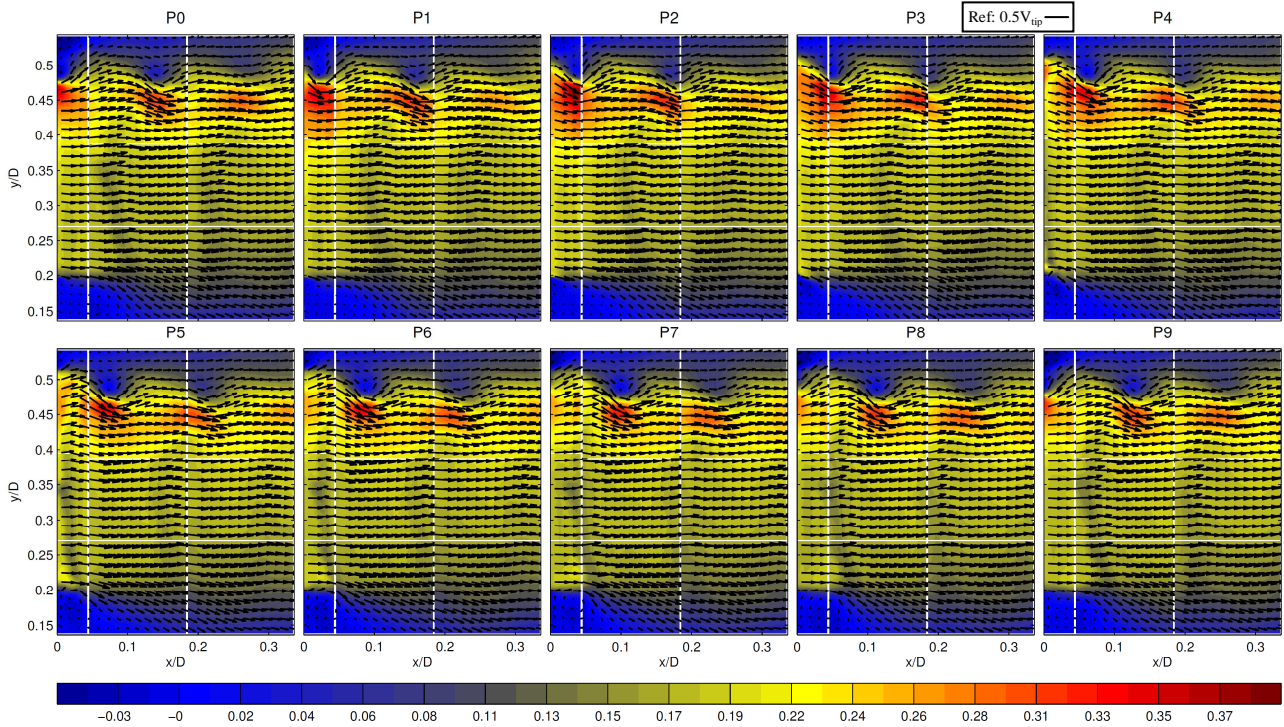


Figure 5: Dimensionless phase averaged axial velocity contour normalized by the tip speed for entire field of view, with velocity vectors diluted by 10 in both directions for clarity. The phases are indicated at the top of each plot.

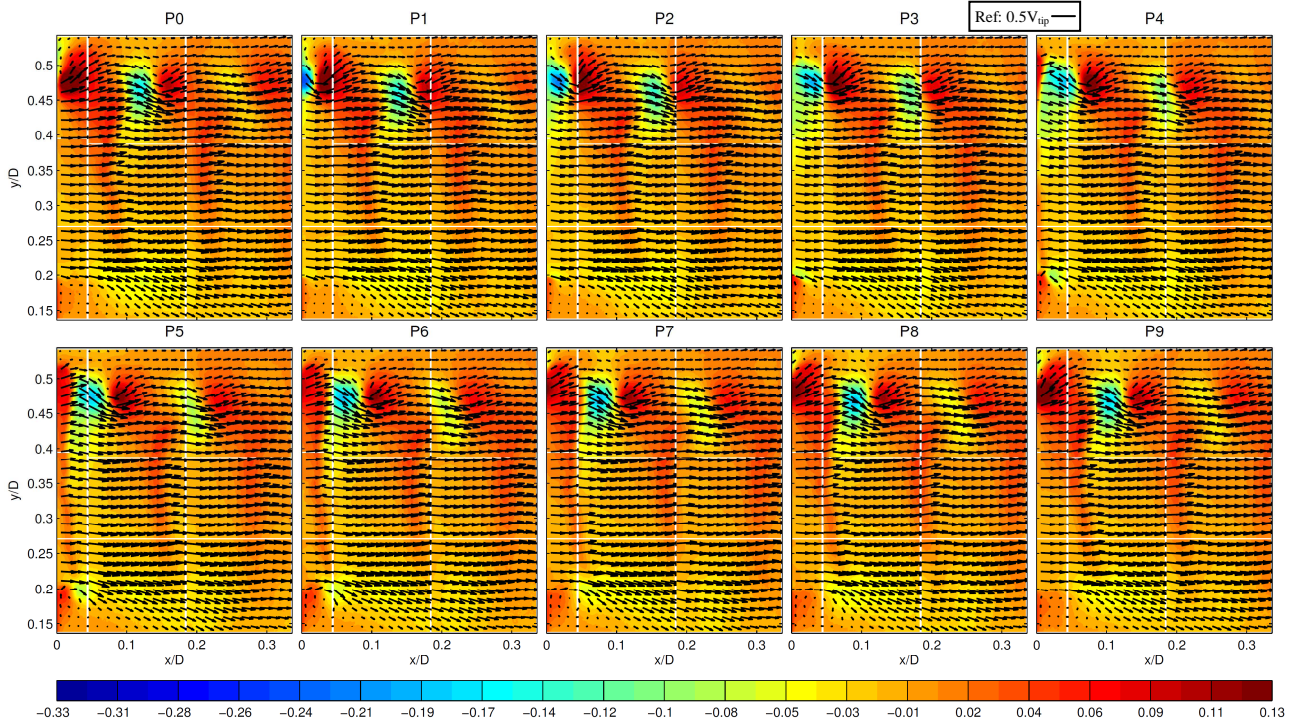


Figure 6: Dimensionless phase averaged radial velocity contour normalized by the tip speed for entire field of view, with velocity vectors diluted by 10 in both directions for clarity. The phases are indicated at the top of each plot.

The positive vorticity streak is much stronger towards hub and mid-span whereas it broadens near the tip and loses intensity. The negative vorticity streak becomes stronger near the tip as the flow induced by the tip vortex pulls the top of this streak radially inward while broadening it

immediately below each vortex. As expected, the vorticity is negative in the low speed separated region behind the fan hub, peaking in the the shear layer extending from the hub corner. The turbulence levels (both components, Fig 7-8) are high in: (i) the tip vortices and the vorticity “sheets” extending from them; (ii) in the separated region behind the blade hub, and in the wake of this hub further downstream, persisting over the entire axial extent of the measurement area; (iii) at the intersection of the blade wakes with the separated region behind the hub, and (iv) to a lesser extent, but still clearly evident, in the blade wakes. As they migrate downstream, the regions with elevated turbulence in the wakes and tip vortices expand and become homogenized, i.e. the spatial variability within them decreases, and the associated peak magnitudes decrease.

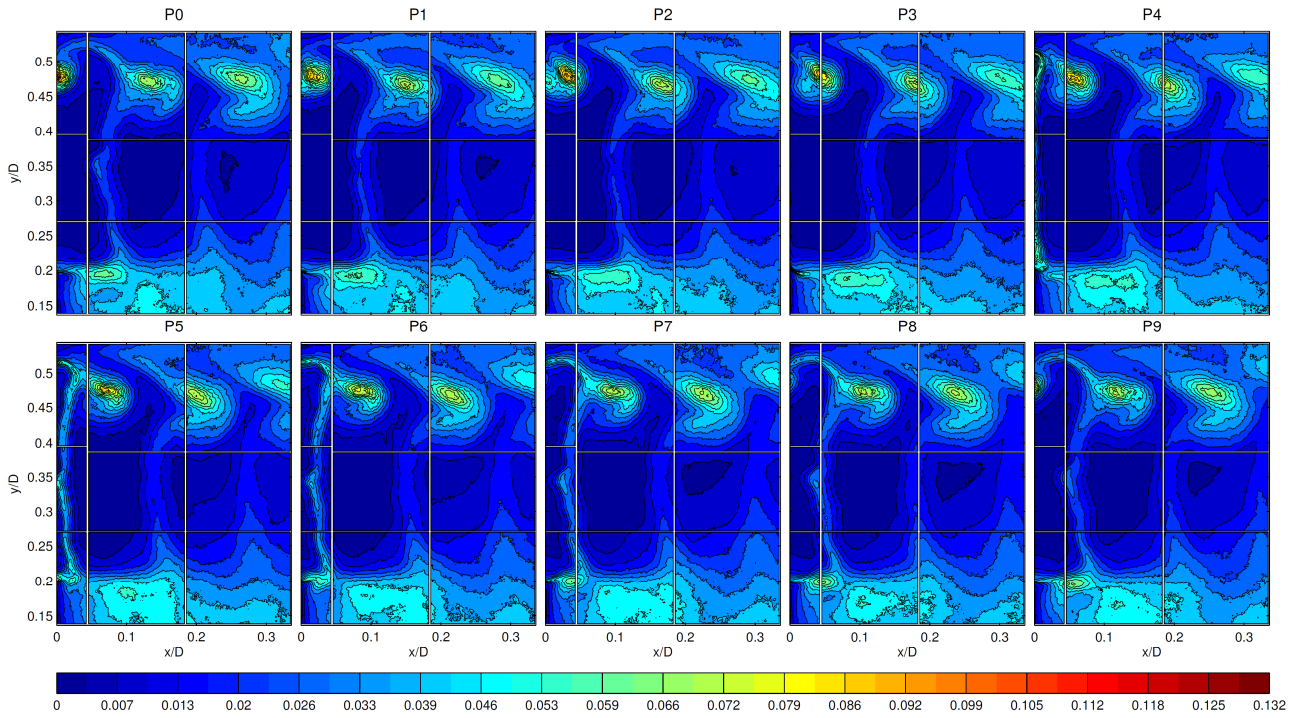


Figure 7: Dimensionless phase averaged axial velocity fluctuation contour normalized with tip speed.

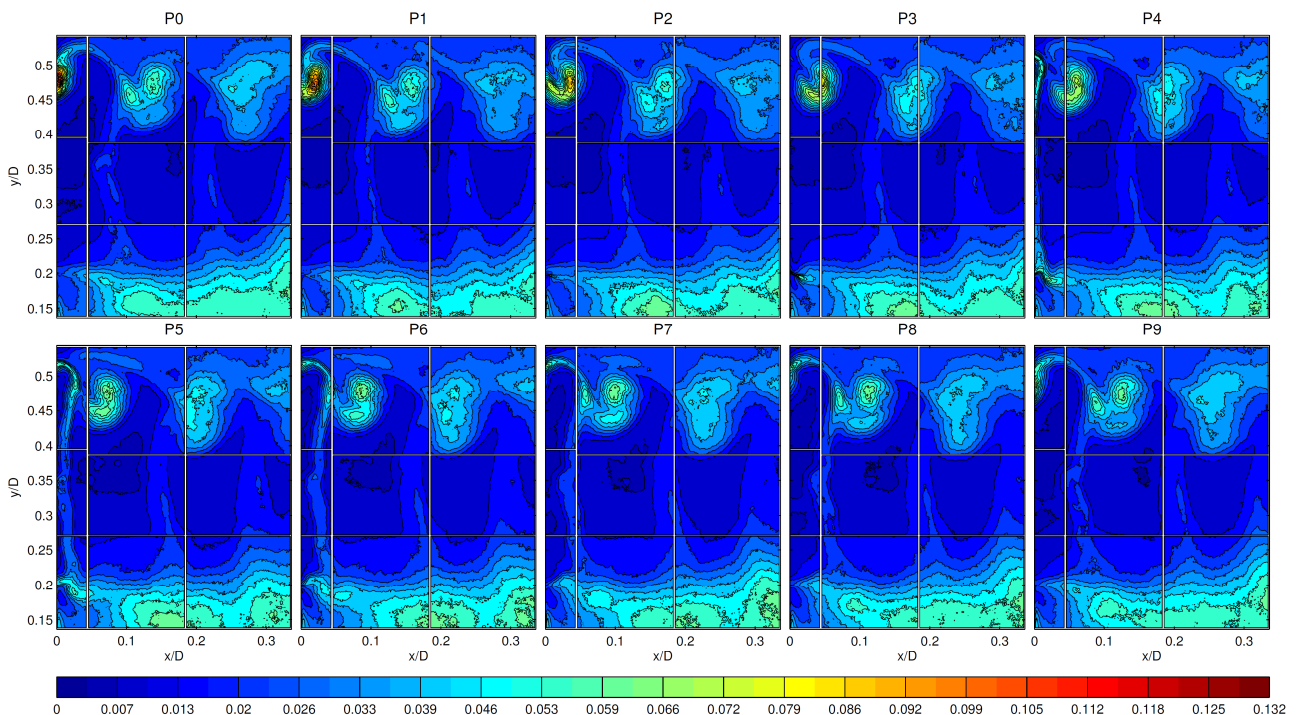


Figure 8: Dimensionless phase averaged radial velocity fluctuation contour normalized with tip speed.

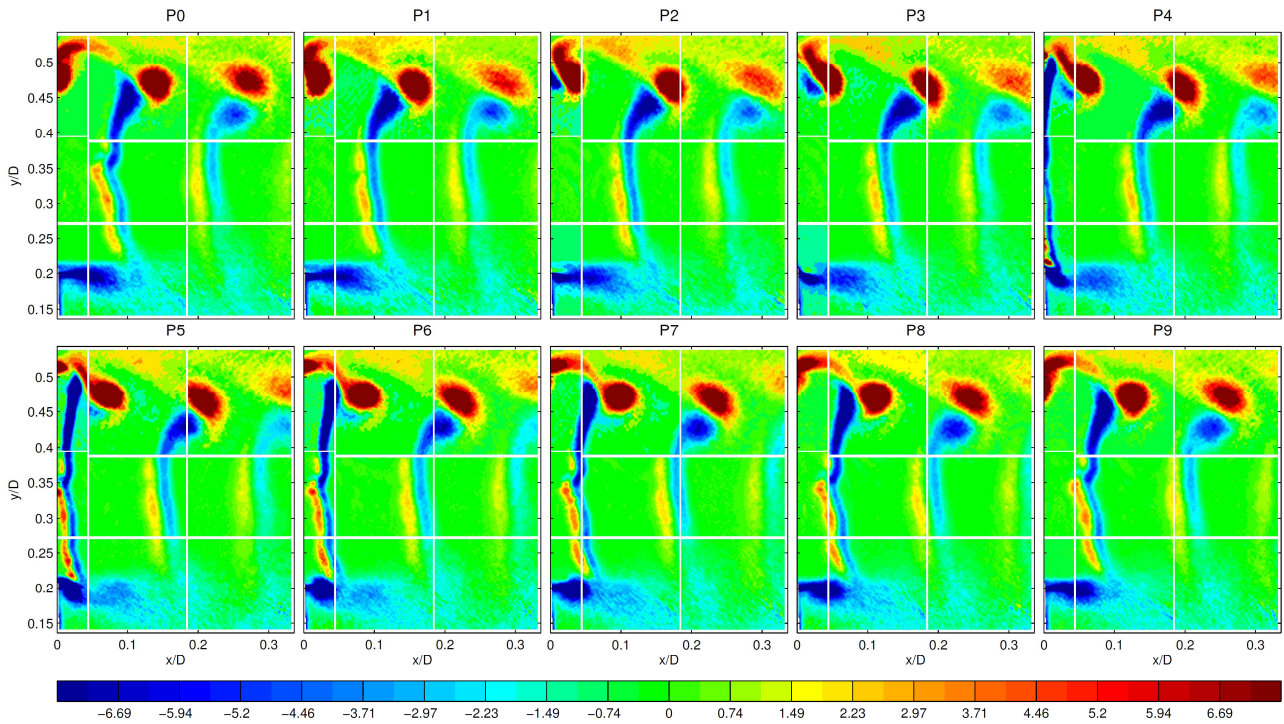


Figure 9: Dimensionless phase averaged circumferential vorticity contour (normalized with shaft rotation speed)

Fig 10 quantifies trends in the magnitude of mean and fluctuating radial velocity at two selected radial locations. The first dissects the tip vortex at $y/D = 0.47$ (Fig 10-a, c) and the second crosses the wakes at mid span: $y/D = 0.33$ (Fig 10- b, d). Results for all blade phases exhibit persistent similarity in profiles as the structures propagate downstream, hence phase P1 is highlighted to illustrate characteristic trends.

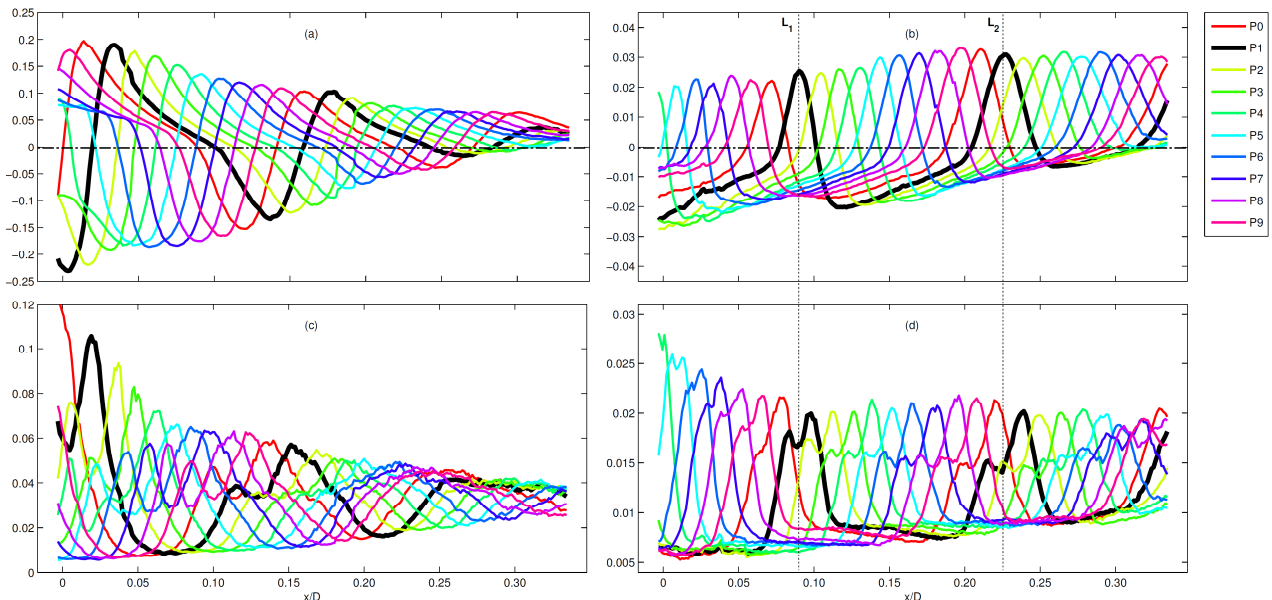


Figure 10: Streamwise profiles of (a) V/V_{tip} at $y/D = 0.47$, (b) V/V_{tip} at $y/D = 0.33$, (c) $\langle v'v' \rangle^{1/2}/V_{tip}$ at $y/D = 0.47$, (d) $\langle v'v' \rangle^{1/2}/V_{tip}$ at $y/D = 0.33$ for all phases. Note the change in vertical scales between plots.

The radial velocity is typically low except for significant oscillations in the immediate vicinity of the tip vortex (Fig 10-a). For phase 1, the tip vortex swirls flow that is bounded by the shroud walls upstream of its center ($x/D < 0.05$), but is free to induce a flow that entrains the unbounded wake of the previous blade, which is located downstream of the center. Consequently, the tip vortex induced vertical velocity distribution is asymmetric, with a sharp vertical velocity gradient ($\partial V/\partial x > 0$)

upstream of the tip vortex, but a much shallower gradient downstream, where $\partial V/\partial x < 0$, e.g. at $0.05 < x/D < 0.1$. As anticipated, regions of high shear persistently have high rms values of velocity fluctuations (Fig 10-c). The fluctuations peak in the $\partial V/\partial x > 0$ region to the left of the vortex center, and have smaller maxima in the $\partial V/\partial x < 0$ region to the right of the vortex. As the tip vortex diffuses downstream, the radial velocity oscillations decay (Fig 10-a), and with them, the corresponding rms intensity (Fig 10-c). As the oscillations diminish, the mean profiles converge to a low positive mean value, indicating a radially outward migration induced presumably by radial pressure gradients.

At mid-span, the mean radial velocity (Fig 10-b) distributions have positive peaks in narrow regions where the blade wakes are entrained by the tip vortices. The entrainment speed is much lower than that occurring in the vicinity of the vortex. As shown earlier (Fig 5, 6), these radial “jets” coincide with the regions having streamwise velocity deficits. The radial velocity peaks decay with x/D , but at a slower rate than those occurring in the tip region. Between the radial jets, V is negative, however, the profiles still converge towards positive radial values i.e. the entire rotor wake is expanding, consistent with the radially outward of structures in the tip region. Lines L_1 and L_2 which coincide with the center of the radial jets (Fig 10-b), are used for demonstrating that the peaks in turbulence levels (Fig 10-d) occur in regions of high velocity gradients on both sides of the jet center. The asymmetry in the magnitude of these peaks is consistent with the lower magnitude of mean velocity gradients ($\partial V/\partial x$) to the left of each jet. The difference in gradient cannot be easily discerned from Fig 10-b, but is evident from the diminishing magnitude of the positive vorticity layer to the left of the jet in Fig 9 in comparison to the persistent negative layer on the right side.

CONCLUSIONS

An optically index matched facility was built for the purpose of measuring the flow and turbulence within and around an automotive fan model. The present high resolution 2D PIV experiments focus on the structures of phase averaged flow and turbulence in the fan wake. The results include distributions of phase averaged axial and radial velocity components for ten different rotor phases covering an entire blade cycle, as well as the corresponding rms values of velocity fluctuations. Distributions of circumferential vorticity help in identifying dominant structures, such as the tip vortices, blade wakes, and separated region behind the rotor hub. Examination of the results leads to the following key observations:

A sample area extending to $x/D=0.33$ covers three generations of the helicoidal system each consisting of a tip vortex containing a concentrated positive vorticity, as well as a blade wake characterized by an axial velocity deficit, positive radial velocity, and parallel layers of vorticity with opposite signs. In addition, the flow field contains a large hub separation region, where the axial velocity is negative and low, followed by a hub wake, which interact with the blade wakes. The turbulence levels are particularly high around the tip vortices, as well as in the shear layer at the edge of the separated region and at the intersections of blade wakes with this shear layer and hub wake downstream. The turbulence level is also elevated within the blade wakes, as expected.

Due to their proximity, positive radial velocity induced by the tip vortex generated by one blade pulls the wake of the previous blade radially outward, creating what appears to be a series of narrow radial jets containing the inherent negative and positive vorticity streaks on either side. The radial velocity fluctuations peak in regions of high $\partial V/\partial x$ on both sides of the jet center. The fluctuations are higher on the side with higher magnitude of $\partial V/\partial x$. The streamwise velocity fluctuations have a broad peak within the wake. The magnitudes of these peaks are also asymmetric, with higher values measured on the side with higher mean streamwise velocity gradients ($\partial U/\partial x$). The oscillations in radial velocity and associated turbulence decay rapidly with downstream distance in the tip region, the streamwise velocity oscillations and associated fluctuations also decay, but at a slower rate.

ACKNOWLEDGEMENTS

This project is partly sponsored by Robert Bosch LLC. We would like to thank Dr. Yury Rhonzes and Stephen King for their immense contributions towards the design, completion and maintenance of the facility. Kaushik Sampath wishes to acknowledge Vignesh Kannan, Aditya Nayak, Pranav Joshi, Cao Zhang, Rinaldo Miorini and other colleagues for their help with the experiment setup and useful discussions.

REFERENCES

- [1] Uzol O, Katz J – *Flow measurement techniques in turbomachinery*, **2007**
- [2] Lakshminarayana B, and Poncet A – *A method of measuring three-dimensional rotating wakes behind turbomachinery rotors*, **1974**
- [3] Lakshminarayana B – *Three-Dimensional Flow Field in the Tip Region of a Compressor Rotor Passage—Part I: Mean Velocity Profiles and Annulus Wall Boundary Layer*, **1982**
- [4] Dong Y, and Cumpsty NA – *Compressor blade boundary layers: Part 2—measurements with incident wakes*, **1990**
- [5] Hsu S., and Wo A – *Near-wake measurement in a rotor/stator axial compressor using slanted hot-wire technique*, *Experiments in Fluids*, 23(5), pp. 441–444. **1997**
- [6] Furukawa M, and Saiki K – *Effects of stream surface inclination on tip leakage flow fields in compressor rotors*. **1998**
- [7] Strazisar AJ – *Investigation of flow phenomena in a transonic fan rotor using laser anemometry*. **1984**
- [8] Zaccaria MA, and Lakshminarayana B – *Unsteady flow field due to nozzle wake interaction with the rotor in an axial flow turbine: Part I: Rotor passage flow field*, *Journal of turbomachinery*, 119(2), pp. 201–213. **1997**
- [9] Woisetschläger J., Mayrhofer N., Hampel B., Lang H., and Sanz W – *Laser-optical investigation of turbine wake flow*, *Experiments in Fluids*, 34(3), p. 371378. **2003**
- [10] Woisetschläger J., and Göttlich E – *Recent Applications of Particle Image Velocimetry to Flow Research in Thermal Turbomachinery*. **2008**
- [11] Raffel M, Willert CE, Wereley ST, Kompenhans J – *Partical Image Velocimetry, a practical guide*, Springer. **2007**
- [12] Miorini RL, Wu H, and Katz J – *The internal structure of the tip leakage vortex within the rotor of an axial waterjet pump*. **2012**
- [13] Uzol O., Chow Y., Katz J., and Meneveau C. – *Unobstructed particle image velocimetry measurements within an axial turbo-pump using liquid and blades with matched refractive indices*. *Experiments in Fluids*, **33**(6), p. 909919. **2002**
- [14] Wu H, Miorini RL, and Katz J – *Measurements of the tip leakage vortex structures and turbulence in the meridional plane of an axial water-jet pump*. **2011**
- [15] Wu H, Miorini RL, Tan D and Katz J – *Turbulence within the Tip-Leakage Vortex of an Axial Waterjet Pump*. **2012**
- [16] Soranna, Francesco, et al. – *The effect of IGV wake impingement on a rotor boundary layer*, *Proceedings of the 44th AIAA Aerospace Sciences Meeting and Exhibit*. **2006**.

- [17] Soranna, Francesco, et al. – *Turbulence within a turbomachine rotor wake subject to nonuniform contraction*. AIAA journal 46.11: 2687-2702. **2008**
- [18] Soranna, Francesco, et al. – *The effects of inlet guide vane-wake impingement on the boundary layer and the near-wake of a rotor blade*. Journal of Turbomachinery 132.4: 041016. **2010**
- [19] Talapatra S, and Katz J – *Three-dimensional velocity measurements in a roughness sub layer using microscopic digital in-line holography and optical index matching*. **2013**
- [20] Hong J, Katz J, and Schultz MP – *Near-wall turbulence statistics and flow structures over three-dimensional roughness in a turbulent channel flow*. **2011**
- [21] Hong, J., et al. – *Coherent structures and associated subgrid-scale energy transfer in a rough-wall turbulent channel flow*. Journal of Fluid Mechanics, 712, 92-128. **2012**
- [22] Bai K, Katz J, and Meneveau C – *Index-Matched PIV Measurements of Turbulence inside a Fractal-Tree Canopy*. **2012**
- [23] Bai, Kunlun, et al. – *Experimental study of spectral energy fluxes in turbulence generated by a fractal, tree-like object*. Physics of Fluids 25.11 (2013): 110810. **2013**
- [24] Cotroni A., Felice F., Romano G., and Elefante M – *Investigation of the near wake of a propeller using particle image velocimetry*. Experiments in Fluids, **29**(7), pp. S227–S236, **2000**
- [25] Morris S., Good J., and Foss J. *Velocity measurements in the wake of an automotive cooling fan*. Experimental Thermal and Fluid Science, **17**(1-2), p. 100106, **1998**
- [26] Yoon JH, and Lee SJ – *Stereoscopic PIV measurements of flow behind an isolated low-speed axial-fan*. **2004**
- [27] Felli M., Felice F., Guj G., and Camussi R. – *Analysis of the propeller wake evolution by pressure and velocity phase measurements*. Experiments in Fluids, **41**(3), pp. 441–451, **2006**
- [28] Roosenboom EWM, Heider A, and Schröder A – *Investigation of the propeller slipstream with Particle Image Velocimetry*. **2009**
- [29] Bai K., and Katz J. – *On the refractive index of sodium iodide solutions for index matching in PIV*. Experiments in Fluids, **55**(4). **2014**
- [30] Budwig R – *Refractive index matching methods for liquid flow investigations*. Experiments in Fluids, **17**(5), pp. 350–355. **1994**
- [31] Roth, Gary I., et al. – *Measurements of the flow structure and turbulence within a ship bow wave*. Physics of Fluids 11.11: 3512-3523. **1999**
- [32] Roth GI, and Katz J – *Five techniques for increasing the speed and accuracy of PIV interrogation*. **2001**
- [33] Westerweel J., and Scarano F – *Universal outlier detection for PIV data*. Experiments in Fluids, **39**(6), pp. 1096–1100. **2005**